Parsons Luke, A (Orcid ID: 0000-0003-3147-0593)
Overpeck Jonathan (Orcid ID: 0000-0002-3843-9313)
Bush Mark, Bennett (Orcid ID: 0000-0001-6894-8613)

Confidential manuscript submitted to Water Resources Research

The threat of multi-year drought in western Amazonia

L. A. Parsons[1], S. LeRoy[2], J. T. Overpeck[3], M. Bush[4], G.M. Cárdenes-Sandí[5], S. Saleska[6]

[1]Department of Geosciences, University of Arizona, Tucson, Arizona 85721, USA.

[2]Institute of the Environment, University of Arizona, Tucson, Arizona 85721, USA.

[3]School for Environment and Sustainability, University of Michigan, Ann Arbor, Michigan 48109, USA

[4]Department of Biological Sciences, Florida Institute of Technology, Melbourne, Florida 32901, USA

[5]Escuela Centroamericana de Geología, Universidad de Costa Rica, 2060 San José, Costa Rica

[6]Department of Ecology and Evolutionary Biology, University of Arizona, Tucson, Arizona 85721, USA

Corresponding author: Luke A Parsons (LukeAParsons@email.arizona.edu)

Key Points:

- We present results from a high-resolution paleoclimate record of hydroclimatic variability in the western Amazon
- Our paleoclimate record suggests western Amazonia has regularly experienced multi-year drought over the last millennium
- Earth system model simulations may underestimate the background risk of multi-year western Amazonian drought

This is the author manuscript accepted for publication and has undergone full peer review but has not been through the copyediting, typesetting, pagination and proofreading process, which may lead to differences between this version and the Version of Record. Please cite this article as doi: 10.1029/2017WR021788

Abstract

Recent "once-in-a-century" Amazonian droughts highlight the impacts of drought and climate change on this region's vegetation, carbon storage, water cycling, biodiversity, land use, and economy. The latest climate model simulations suggest this region will experience worsening future drought. However, the instrumental record is too short to quantify the range of background drought variability, or to evaluate extended drought risk in climate models. To overcome these limitations, we generated a new, highly resolved lake record of hydroclimatic variability within the western Amazon Basin. We find that Amazonia has regularly experienced multi-year droughts over the last millennium. Our results indicate that current climate model simulations likely underestimate the background risk of multi-year Amazonian drought. These findings illustrate that the future sustainability of the Amazonian forest and its many services may require management strategies that consider the likelihood of multi-year droughts superimposed on a continued warming trend.

Plain Language Summary

The Amazon basin recently experienced multiple "once-in-a-century" droughts that impacted the region's water cycle, economy, vegetation, and carbon storage. However, the instrumental record in this region tends to be too short to determine if these droughts are abnormal in a long-term context. Paleoclimate data can extend drought records that help water and land managers plan for these events in the face of climate change. To provide additional information about pre-instrumental drought, here we present results from a new paleoclimate lake record based on sediments we recovered from Lake Limón in the Peruvian Amazon. We find that concentrations of elements in the Lake Limón sediment cores are likely recording past changes in rainfall variability. We use this elemental variability to generate a new, millennial-length record of drought for the western Amazon. We show that this region has experienced multi-year droughts at least twice a century over the last ~1400 years. The frequency and severity of these paleoclimate-inferred droughts may exceed most climate model and instrumental-era drought risk estimates. Our findings illustrate that the future sustainability of the Amazonian forest and its many ecosystem services may require management strategies that consider the likelihood of multi-year droughts in addition to continued warming.

1 Introduction

The Amazon rainforest is a biodiversity hotspot (Mittermeier et al., 1998) and a potential tipping element of the Earth system that provides critical ecosystem services both locally and globally (Malhi et al., 2008; Lenton et al., 2008). Ecosystems within the Amazon basin provide a habitat for up to a quarter of the world's terrestrial species (Dirzo and Raven, 2003), and Amazonian plants and soils hold the equivalent of approximately half of the carbon contained in the pre-industrial global atmosphere (Malhi et al., 2008; Gloor et al., 2012). Furthermore,

evapotranspiration in this region helps drive regional and global atmospheric circulation (Malhi et al., 2008).

The future composition of the Amazonian rainforest, and thus its ability to provide these ecosystem services, depends on land use and the background climate (Nepstad et al., 2009; Malhi et al., 2009). The prospect of large-scale Amazonian forest dieback, in which rangeland or savanna replaces forest, has focused attention on the importance of long-term drought in Amazonia (Cox et al., 2004; Lewis et al., 2011; Malhi et al., 2009). Although the Amazonian forest persisted during moderate drought in the recent past (Bush et al., 2016), it is uncertain if future climate change and other anthropogenic stressors will trigger rapid forest dieback in this 'climate change hotspot' (Davidson et al., 2012; Diffenbaugh and Giordi; 2012). Decreased seasonal precipitation and warming are already contributing to drought and vegetation stress in this region (Lewis et al, 2011; Dai, 2013; Jimenez-Munoz et al., 2016; Saatchi et al., 2013). Although future warming will lead to evaporation increases (Dai, 2013), the duration of precipitation extremes combined with this warming will likely drive a large portion of ecosystem stress, and thus control much of this region's carbon storage (Tian et al., 1998; Phillips et al., 2009). Reduced rainfall alone can increase the risk of fire and forest dieback, which can in turn lead to drought intensification, self-amplified forest loss, and possibly a deforestation-induced tipping point (Brando et al., 2014; Zemp et al., 2017; Boers et al., 2017).

Given the possibility that future extreme drought events could destabilize parts of the Amazonian forest (Zemp et al., 2017), it is critical to understand the future range of drought this vegetation might have to endure. Instrumental and satellite-based climate records for Amazonia only span the last few decades, highlighting the need for high-resolution paleoclimate records to extend our knowledge of past climate further back in time. To overcome this limitation, we have generated a ~1400-year paleohydrological record using sediments from a rare lowland lake in western Amazonia.

Lake sediments can provide high-resolution archives that can be used to study catchment-scale to regional-scale environmental change over a range of time periods, from seasons to millennia (Cohen, 2003; Davies et al., 2015). Specifically, paleoclimate lake records have been used to reconstruct pre-instrumental hydroclimatic variability in various regions around the world. For example, Shanahan et al. (2009) reconstructed past drought variability in West Africa using oxygen isotopes and high-resolution µ-x-ray fluorescence (µ-XRF) scans of laminated sediments from Lake Bosumtwi. In the Americas, Bird et al. (2011) used oxygen isotopes from Laguna Pumacocha sediments in the Central Peruvian Andes to reconstruct past South American monsoon variability. Similarly, Haberzettl et al. (2005) reconstructed past climate variability in southern Argentina, and Metcalfe et al. (2010) inferred past changes in the northern Mexican monsoon from XRF scans of sediments.

We expand on recent decades of high-resolution µ-XRF research (review by Davies et al., 2015) to develop a highly resolved record of hydroclimatic variability in western Amazonia. We compare our paleohydrological record to a variety of paleoclimate records from tropical South America and to background drought risk in transient climate simulations driven by full

natural and anthropogenic forcings (Schmidt et al., 2012) to better quantify the range of drought variability and evaluate extended drought risk in climate models.

2 Materials and Methods

2.1 Core retrieval and study area

Lake Limón (6˚43'S, 76˚14'W; 600 m above sea level) is located in north-central Peru at the base of the eastern flank of the Andes Mountains on the western edge of the Amazon Basin (Fig. 1a). Lake Limón (~535m in length, ~80m in width, ~13.6m in depth) lies in a small, crescent-shaped basin with one small, hypersaline stream entering and exiting the lake (Fig. 1b). The clay-rich hillsides surrounding the lake primarily consist of highly eroded sedimentary rocks. Anoxic waters below ~5m depth inhibit bioturbation of lake-bottom sediments and help to preserve finely laminated sediments (Fig. S1).

In 2009, we retrieved three piston cores (denoted LP-1 to LP-3), 4-5 m in sediment length from Lake Limón at a water depth of ~13m (Fig. 1c). We also retrieved six gravity cores (denoted LU-1 to LU-6) taken from within 50 m of the piston cores that captured the mud-water interface with minimal mixing. We extruded the top portion of each core at 2.5 mm increments to prevent mixing during transport. For this study, we produced a composite of LP-3 (4.8 m long) and LU-5 (1.2 m long taken at 12.2 m depth; Fig. 1c) by correlating the two cores where they overlap using both lithologic and chemical tie points (Fig. S1). Here we have chosen to only analyze Lake Limón data preceding 1972 CE because the extruded sediments at the top of the core were too flocculent to conduct similar analyses to the lower sediments.

2.2 Dating of sediments and age model

We constructed an age model for the Lake Limón cores using 21 radiocarbon (^{14}C) dates on terrestrial plant material and 12 ^{210}Pb measurements on the uppermost sediment in the gravity core (Table S1, Fig. 2). We excluded three ^{14}C dates because there was too little carbon to obtain an accurate date. We also excluded two dates taken on leaves that resulted in outliers implying the leaves were perhaps re-deposited from shallow areas of the lake (Table S1).

Pretreatment for radiocarbon samples was performed using the standard acid-base-acid procedure of HCl and NaOH to remove any carbonates and humic acids (Hedges et al., 1989). The samples were then combusted at the University of Arizona Accelerator Mass Spectrometry (AMS) facility. Twelve additional samples, taken at 20 mm intervals from the top of the gravity core (including extruded sediment), were sent to The Florida Institute of Paleoenvironmental Research (FLIPER) laboratory at The University of Florida for ^{210}Pb and ^{137}Cs activity measurement. ^{210}Pb ages were calculated using the constant rate of supply model (Appleby,

2002; Appleby and Oldfield, 1983). Measured ^{137}Cs values were extremely low and were thus not included in the age model.

The age model was constructed using a non-Bayesian, 'classical' age-depth model program known as *clam* (Blaauw, 2010). This software first calibrates ^{14}C dates using the SHCal04 calibration dataset, then produces a "best fit" age model using a LOESS smooth curve function through both ^{210}Pb and ^{14}C dates (McCormac et al., 2004). After all age reversals were removed, over 1000 iterations remained to produce the final age model (Fig. 2).

2.3 Elemental analysis

We sampled the Lake Limón sediment using well-established µ-x-ray fluorescence (µ-XRF) methods (e.g., Niemann et al., 2009; Moreno et al., 2007; Shanahan et al., 2008, 2009). We took thin-sections from both gravity and piston cores then performed acetone exchanges to remove water in the sediment. We embedded the sediment in resin using standard procedures to reduce noise due to water formation and surface roughness during µ-XRF measurements (Pike and Kemp, 1996). We measured the elemental abundances of 10 elements (Al, Si, S, K, Ca, Ti, Mn, Fe, Rb, and Sr) using an EDAX Eagle III tabletop scanning µ-XRF analyzer at the University of Arizona (Shanahan et al., 2008).

We used rotated empirical orthogonal functions (EOF, also known as principal components analysis, or PCA; e.g., North et al., 1982) to determine the primary modes of variability in 10 elemental time series (Balascio et al., 2011; Shala et al., 2014). We removed the linear trend and normalized all elemental time series before conducting EOF analysis (Fig. S2). To normalize the elemental time series prior to EOF analysis, we compared two methods and found minimal changes in our results: (1) remove the mean and divide by the standard deviation ('z-score'), (2) employ a modified inverse Rosenblatt transform to 'gaussianize' the data (Van Albada and Robinson, 2007). When we compared Lake Limón principal component one (PC1) to other time series (Table 1), we binned the data due to age model uncertainty and accounted for the associated reduced degrees of freedom in our significance testing.

Many lake sediment XRF studies use elemental ratios to infer past environmental variability (e.g., Davies et al., 2015), but 'single element' XRF studies, in which elemental ratios are not employed, are also common (e.g., Shanahan et al., 2009; Finkenbinder et al., 2014; Balascio and Bradley, 2012; Matthews-Bird et al., 2017). In this analysis, we use single-element counts (not elemental ratios) to calculate PC1. In Lake Limón, PC1 is strongly driven by Ti, which is generally interpreted to be a proxy for runoff and erosion (allochthonous input). Previous XRF-based studies of lake sediments have found that single-element Ti abundance is associated with catchment runoff (Haberzettl et al., 2005; Metcalfe et al., 2010; Balascio and Bradley, 2012; Matthews-Bird et al., 2017).

2.4 Charcoal analysis

Sediment subsamples of 0.5cm^3 were removed for charcoal analyses at 5cm depth intervals (77 samples spanning ~560-1972CE). Samples for charcoal analysis were gently disaggregated in 10% KOH then sieved at 60 and 180 μm. The retained fraction was placed in a petri dish and the charcoal particles were identified and quantified under a stereomicroscope (Clark and Royal; 1996). All charcoal values are reported as counts of charcoal fragments per 1cm^3. Charcoal data are shown here in 40-year bins to account for any possible age model uncertainty between sediment cores.

2.5 Power spectra estimation in paleoclimate and climate model data

We could not directly compare the time evolution of Coupled Model Intercomparison Project Phase 5 (CMIP5) and paleoclimate time series due to the uncertainties associated with external forcing, unknown initial conditions, and the independent evolution of internal variability. Instead we compared simulated and observed records in the frequency domain. We used previously established methods (Ault et al., 2013) to calculate and analyze the variance spectra of precipitation CMIP5 Last Millennium ('past1000') (Schmidt et al., 2012) and CMIP5 pre-industrial control model simulations (Taylor et al., 2012), as well as multiple hydroclimate-sensitive paleoclimate records from around tropical South America (Table 1).We used the Lomb-Scargle method (Lomb, 1975; Scargle, 1982) to estimate the power spectra in both paleoclimate as well as climate model data; this technique is often employed with unevenly sampled paleoclimate data. We normalized all time series by removing the mean and dividing by the standard deviation of the full time series ('z-score') before performing spectral analysis. We limited our analysis to paleoclimate and model data for the time period 850-1850CE to exclude any significant influences of anthropogenic climate change. We calculated climate model precipitation spectra from model grid boxes closest to Lake Limón in western Amazonia (8ºS-5ºS, 77ºW-73ºW) and also for the Amazon basin (12ºS-3ºN, 72ºW-48ºW) to test if simulated precipitation variability was sensitive to its proximity to the Amazon-Andes transition zone.

2.6 Drought assessment

CMIP5 simulated precipitation drought lengths were calculated from model grid boxes closest to Lake Limón in western Amazonia (8ºS-5ºS, 77ºW-73ºW). Lake Limón-inferred droughts were calculated over 850-1850CE to overlap with model data. Droughts were defined as a unique instance when the 5-year running mean of the time series crossed the threshold one standard deviation (-1σ) or two standard deviations (-2σ) below the long-term mean (850-1850CE).

3 Data

3.1 Gridded Instrumental-Based Data

We compared 1ºx1º degree resolution gridded GPCCv7 precipitation over tropical South America to NOAA ERSSTv4 tropical North Atlantic and tropical Pacific sea-surface temperatures (SST) to study the drivers of interannual hydroclimatic variability during the time period 1901-2014CE (Schneider et al., 2014; Huang et al., 2015) (Fig. 3). We also compared Lake Limón principal component data to gridded GPCCv7 precipitation (~1901-1972CE overlap) and NOAA ERSSTv4 SST (~1854-1972CE overlap) data. We show the climatological mean satellite-era September to March South American precipitation from the GPCP v2.3 dataset in Figure 1a (Adler et al., 2003).

3.2 Climate Model Data

We estimated drought frequency and duration as well as power spectra from CMIP5 pre-industrial control and Last Millennium climate model output (Taylor et al., 2012; Schmidt et al., 2012). We conducted our analysis on all CMIP5 models with at least 500 years of data that did not show a global mean temperature trend of greater than 1°C/millennium in the control run ($N_{past1000}$=10, $N_{control}$=28).

3.3 Paleoclimate and River Gauge Data

We also compared our Lake Limón time series to a variety of tropical South American paleoclimate data and one Amazonian river gauge station. Table 1 includes data types, citation information, locations, correlations with Lake Limón principal components, and time span of these records. We included all tropical South American hydroclimate-sensitive paleoclimate data (at sub-decadal resolution) available on the NOAA Paleoclimate website at the time of analysis. All correlation coefficients were calculated using 5-year bins except Cariaco SST and Ti, which were binned into 10-year bins. Correlation coefficients at the 95% confidence interval are shown in bold italics and coefficients at the 90% confidence interval are shown in bold (Table 1). Effective sample sizes were used to account for autocorrelation. Locations of South American paleoclimate records are shown in Figure 1a.

4 Results and Discussion

4.1 Local climate

Although evapotranspiration within the Amazonian basin can drive much of the local hydrological cycle and atmospheric circulation, tropical SSTs, both in the tropical Pacific and

North Atlantic Oceans, affect Amazonian precipitation on seasonal and longer timescales (Fig. 3) (e.g., Espinoza et al., 2016; Marengo and Espinoza, 2016). SST anomalies in both ocean basins have helped cause seasonal drought in parts of Amazonia during the instrumental era (Marengo and Espinoza, 2016). Tropical North Atlantic SST has a strong influence on rainfall across southern and western Amazonia (Lewis et al., 2011; Yoon and Zeng, 2010; Marengo and Espinoza, 2016). Warmer waters north of the equator in the tropical Atlantic draw the rainfall belt northward, leading to convergence north of the equator and subsidence over southern and western Amazonia (Cox et al., 2008). Eastern tropical Pacific SST has a stronger impact on precipitation in northern, central, and eastern Amazonia (Jimenez-Munoz et al., 2016; Ronchail et al., 2002). Here we are specifically interested in the oceanic drivers of interannual rainfall anomalies; our analysis of SSTs and GPCCv7 precipitation data suggests that tropical North Atlantic SSTs appear to drive much of the rainfall near Lake Limón (Fig. 3). On multi-year timescales, the tropical Pacific shows a weak and geographically inconsistent relationship with rainfall in Peruvian Amazonia (Fig. 3b).

Mean monthly temperatures near Lake Limón exhibit a limited annual range of ~2ºC, and annual precipitation has a bimodal distribution that closely follows the seasonal migration of the tropical rainfall belt and the South American Monsoon System (SAMS) (Correa-Metrio et al., 2010). Precipitation is highest in austral spring to fall, when surface heating is strongest over northern Peru and the surrounding region. In spring, precipitation over Lake Limón peaks as the tropical rainfall belt migrates to the south over northern Peru, and precipitation peaks again in austral fall as the rainfall belt migrates back over the region from the south to north (Vera et al., 2006; Zhou and Lau, 1998).

4.2 Lake Limón elemental variability

We conducted rotated EOF analysis to determine the primary modes of sediment elemental variability (Table 2, Fig. S2). We find that Principal Component 1 (PC1) explains the most variance (40%) and is positively correlated with the abundance of the terrestrial elements Al, K, Ti, Fe and Rb, and negatively correlated with Ca abundance (Table 2). Positive values reflect strong inputs of terrestrial elements (e.g., Ti) and low abundances of Ca (e.g., Finkenbinder et al., 2014; Balascio and Bradley, 2012; Matthews-Bird et al., 2017). PC1 is correlated with instrumenal SST and precipitation variability (Fig. 4). Although PC2 is weakly correlated with instrumental records, the relationships are non-significant, so we do not further discuss them here (Table 1).

Elevated abundances of terrestrial elements, such as those driving PC1, can indicate lower lake level (through an increase in the amount of erodible material as the shoreline approached the lake center during periods of low water level), or increased transport (via runoff). The steep bathymetric profile of Lake Limón suggests that lower lake levels would not significantly impact grain size in the center of the lake because changes in lake level would not

considerably change the distance from the shoreline to the center of the lake (Fig. 1c). The closest shorelines to the coring locations are located above the steepest portions of the lake bottom, supporting our assertion that lake level changes would not appreciably change the proximity of the coring location to the nearest shoreline (Fig. 1c). Furthermore, low-resolution grainsize analysis on the most recent ~600 years of sediment shows little to no relationship with PC1, suggesting that increased grainsize from shifting shoreline location did not consistently play a role in driving PC1 variability (Fig. S3). We have estimated lake volume changes and associated shoreline changes with sequential 1m volume losses and find that each 1m loss of lake depth would change lake volume ~8-10% (Table S2), and a lake volume loss of ~25% would not appreciably shift the shorelines closest to the coring locations (Fig. S4).

$CaCO_3$ normally precipitates under drier conditions; increased Ca drives PC1 in the opposite direction as the terrestrial elements, indicating that PC1 is recording increased transport (wetter) versus higher $CaCO_3$ (drier) conditions in the basin around Lake Limón (Cohen, 2003). We do not think this lake system is calcium starved because of the relatively high Ca concentration in the water column (Table S3). X-ray diffraction (XRD) analysis of the upper sediments in the core suggests that calcite is the dominant Ca-containing mineral present in the sediments, supporting our interpretation of the Ca signal in the sediments (Table S4). We thus have confidence that the PC1 signal is primarily a relative wet/dry (precipitation) signal.

4.3 Instrumental record comparison

Direct comparison of PC1 with gridded instrumental climate observations confirms that the Lake Limón elemental proxy record is sensitive to hydroclimatic variability. Lake Limón PC1 is significantly correlated with wet-season GPCCv7 precipitation (Schneider et al., 2014) (September-March, $r=0.65$, $p<0.02$, 72-year overlap; 5-year bins account for proxy age-model uncertainty) in western Amazonia (Fig. 4a, Fig. 5a). However, precipitation in the Amazon Basin is spatially heterogeneous and observations of precipitation tend to be relatively short and sparse. Additionally, there are no instrumental rainfall records near Lake Limón before ~1950CE.

Due to the lack of consistent rainfall data, we also compared the Lake Limón PC1 directly to SST anomalies, which play a role in driving hydroclimatic variability in Amazonia (e.g., Espinoza et al., 2011; Espinoza et al., 2016; Marengo and Espinoza, 2016; Li et al., 2011). We find a weak, non-significant relationship among Lake Limón principal components and tropical Pacific SST on interannual timescales (5ºS-5ºN and 170-120ºW; 119-year overlap; 5-year bins; Table 1). We also compare Lake Limón PC1 with tropical North Atlantic SST data (5-22ºN and 80-30ºW; 119-year overlap; 5-year bins); the tropical North Atlantic is closely related to anomalous migration of the tropical rainfall belt in the American Tropics and associated droughts in Amazonia (Yoon and Zeng, 2010; Espinoza et al., 2011; Fernandes et al., 2015). The Lake Limón PC1 time series is significantly correlated with tropical North Atlantic SSTs ($r = -0.59$, $p < 0.01$; Fig. 4b, Fig. 5a). Significant spatial correlation during the instrumental era

between tropical North Atlantic SSTs and gridded station-based rainfall data in the Peruvian Amazon confirms that tropical SSTs in this region have been a recent driver of southern and western Amazonian hydrologic variability on interannual to decadal timescales (Fig. 3a; Fernandes et al., 2015). This tropical North Atlantic SST-Peruvian Amazon precipitation relationship remains robust during the more recent satellite era as well (not shown). Thus, multiple lines of evidence (modern North Atlantic-western Amazonia rainfall teleconnection pattern, the relationship between PC1 and tropical North Atlantic SST, and the relationship between PC1 and observed western/southern Amazonian precipitation) suggest that Lake Limón provides a useful proxy record of past hydroclimatic variability in western Amazonia.

4.4 Drought analysis

Based on the evidence outlined above, we use our ~1400-year Lake Limón record of elemental abundance to study pre-instrumental hydroclimatic variability. We identify 31 dry periods in which elemental abundance, which we interpret as a proxy for western Amazonian precipitation, was at least one standard deviation below the mean and 15 periods in which it was at least two standard deviations below the mean (Fig. 5). These inferred droughts range in estimated length from 1 to 24 years with a mean of 7 years (Fig. 6). We also find 26 pluvials in which precipitation was at least one standard deviation above the mean; the longest wet period may have lasted as long as ~80 years (~1290-1370 CE).

These results should be considered with two important caveats. Although a comparison between Lake Limón PC1 and local precipitation (5-year bins) indicates these time series are well-correlated, their distributions are not identical, suggesting there may be a large amount of noise in the PC1 hydroclimatic signal (Fig. 4c). Therefore, a 1-sigma departure from the mean in Lake Limón PC1 likely does not indicate that local precipitation has experienced a 1-sigma 'drought', but rather a relative dry period. Additionally, the Amazon-Andes transition zone in western Amazonia experiences highly heterogeneous rainfall (e.g., Espinoza et al., 2015), and the region showing a significant relationship between local GPCCv7 precipitation and Lake Limón PC1 (Fig. 4a) is confined to a small area within Peru, so these results should be extrapolated cautiously beyond the Peruvian Amazon.

Furthermore, the Lake Limón sediment record is not annually resolved (e.g., by annual varves), but sediment accumulation rates appear to have changed slowly over the last 1400 years (Fig. 2). Our estimates of drought duration are based on these slowly changing mean rates. This approach may underestimate drought durations in western Amazonia given the likelihood that sedimentation slowed during dry periods due to decreased terrigenous element input offset by modest increases in more evaporitic elements (e.g., Ca). Similarly, our record may overestimate the duration of pluvial periods due to higher sediment accumulation rates during wet periods.

4.5 Charcoal, human occupation, and drought

Occupation of this basin by humans would have been limited by the saline lake water, but a long history of occupation at neighboring Lake Sauce, about 2 km to the east (Bush et al., 2016), would have ensured some human influence on the catchment. The presence of charcoal in Lake Limón sediments, almost certainly attributable to human activity, supports our interpretation of PC1 (Fig. 5b). Until ~1500CE, the catchment likely experienced fire followed by erosional events (wet periods) that washed both sediment and charcoal into the lake, causing a peak in both PC1 and charcoal count (e.g., Colombaroli and Gavin, 2010). Elevated charcoal counts during the 14th century confirm that the region experienced extensive erosion during this extended pluvial. Following this wet event, there are fewer charcoal peaks, suggesting a lack of significant human impact in the catchment after ~1500CE, a finding corroborated by charcoal and pollen counts in Lake Sauce (Bush et al., 2016) and a possible regional collapse of local indigenous cultures following European contact. Although the presence of charcoal during certain time periods tends to coincide with data from Lake Sauce, the interpretation of the charcoal results from Lake Limón have certain limitations. For example, the presence of charcoal is often interpreted as an indicator of fire and/or human occupation. It is possible that humans intermittently occupied the basin around Lake Limón, creating periods of intermittent charcoal production relatively unrelated to pluvial activity. However, the saline inlet to the lake suggests that the lake water would have remained relatively salty (and thus likely unusable as a drinking water or irrigation water source), even during relatively wet intervals.

4.6 Comparing paleo-inferred and simulated hydroclimatic variability

The latest CMIP5 model projections indicate that much of Amazonia will experience a trend of decreasing precipitation over the 21st century, and decreased soil moisture as temperatures continue to increase (Christensen et al., 2013; Diffenbaugh and Giorgi, 2012; Jimenez-Munoz et al., 2016). The potential for future multi-year drought in the region is particularly troubling in context of the warming and drying trend that is leading to increasingly hot and severe drought in the region (Jimenez-Munoz et al., 2016). However, many CMIP5 models show a dry bias over Amazonia (e.g., Yin et al., 2013). Furthermore, previous studies have shown that many CMIP5 models underestimate decadal to centennial hydroclimatic variability in many regions of the globe, and these models may underestimate the risk of severe drought in Amazonia (e.g. Ault et al., 2012; 2014). Here, we test this hypothesis with our new 1400-year Lake Limón record (Fig. 7) and with other hydroclimate-sensitive records from tropical South America (Fig. 1a; Table 1).

Whereas Lake Limón PC1 hydroclimatic variance increases from interannual to centennial timescales, CMIP5 precipitation variance is more uniform across timescales (e.g., Parsons et al., 2017), indicating that these models simulate less low-frequency variability in western Amazonia than we observe in our record (Fig. 6; Fig. 7). This mismatch cannot be explained by a problem with model resolution at the Amazon-Andes transition zone (e.g., Guimberteau et al., 2013; Yin et al., 2013) because we find similarly ‘white’ simulated

precipitation spectra across much of tropical South America in most CMIP5 models (Fig. S5) (Parsons et al., 2017). These results suggest that CMIP5 models may underestimate the risk of decadal and longer droughts, and generally underestimate past large-scale shifts in precipitation over South America that have been inferred from the paleoclimate record (e.g., Rojas et al., 2016).

The spectra calculated from other hydroclimate-sensitive paleoclimate records from near or within the Amazon Basin support our finding that hydroclimatic variance increases with timescale (Fig. 7; Fig. S6). Paleoclimate records in the region all agree that hydroclimate varies more strongly over multi-decadal to centennial scales than over interannual to decadal scales. Although formation processes in certain paleoclimate records may smooth much of the sub-decadal hydroclimatic variability (Dee et al., 2017), these processes typically decrease interannual variability and do not increase low-frequency variability, so the low-frequency variability observed in these records may be a real part of the climate system.

Many hydroclimate-sensitive paleoclimate records around tropical South America tend to agree on periods of multidecadal-centennial scale variability (e.g., Bird et al., 2011; Vuille et al., 2012; Apaestegui et al., 2014). For example, multiple $\delta^{18}O$ records indicate the South American monsoon experienced changes during the so-called 'Medieval Climate Anomaly' and 'Little Ice Age,' but the interannual-decadal details of these records often do not agree (e.g., Novello et al., 2016). Dating uncertainties and noise unrelated to regional climate signals in paleoclimate data can limit interpretation of these records, and the Lake Limón record is no exception (Fig. 8). For example, although the Brazilian Pau d'Alho cave $\delta^{18}O$ variability (Novello et al., 2016) shows some general similarities to Lake Limón PC1 ~1200-1600CE, this agreement does not continue throughout the time overlap between the two records (Fig. 8c). Similarly, the Cascayunga $\delta^{18}O$ (Reuter et al., 2009), Cariaco basin (Haug et al., 2001), and Palestina cave δ18O (Apaestegui et al., 2014) variability show inconsistent similarities to Lake Limón PC1 (Fig. 8; Table 1). Regardless of this disagreement, all of these records show relatively 'red' spectra, suggesting that either background hydroclimatic variability in this region is similarly 'red', all of these paleoclimate records are recording non-climatic red noise in different ways, or we are misinterpreting the signals from these paleoclimate records (Fig. S6).

5 Conclusions

Our paleo-model comparison indicates that there is a low-frequency disagreement between simulated and paleoclimate-inferred hydroclimatic variability around tropical South America. If we are correctly interpreting the signals from these paleoclimate records, then the latest Earth system models used to estimate future drought risk in Amazonia underestimate the background risk of prolonged drought (see Fig. S7 for drought distributions of individual CMIP5 models). The Amazonian Lake Limón record supports this finding, as do other paleoclimate records in South America (Fig. S6) and elsewhere (e.g., Ault et al., 2013). The latest Earth system models simulate a western Amazonian drought approximately once per century in the last

millennium (~850-1850CE), but the Lake Limón record indicates this region has experienced an average of at least two droughts per century over the same time period. CMIP5 models show similar hydroclimatic variability across the entire Amazon basin (e.g., Parsons et al., 2017), so this paleo-model mismatch likely cannot be explained by model resolution in the Amazon-Andes transition zone. Moreover, the general pattern of increasing hydroclimatic variance with timescale observed in paleoclimate records indicates that even longer multi-decadal droughts can occur, and that this possibility should be taken into account in climate adaptation planning; this is also a hypothesis that needs to be tested with annually-resolved hydroclimatic records that are even longer than our Lake Limón record. The Lake Limón hydroclimate record provides resource managers with an extended observational basis for estimating future risk of multi-year and longer drought; the updated drought risk estimate based on Lake Limón data is greater than the risk inferred from the short instrumental records or the latest Earth system models.

Proponents of forest management strategies, such as REDD+, should take note that natural variability alone can generate periods of below-average precipitation significantly longer than the seasonal droughts that have occurred in the recent instrumental period. Even recent seasonal droughts have led to increased fire frequency; in the Brazilian Amazon, 21st century droughts have increased fire incidence and associated carbon emissions, despite declines in deforestation rates (Aragão et al., 2018). Although the forests persisted through multiple inferred dry periods from the Lake Limón record over the last ~1400 years, their resilience may be undermined in the future by non-climatic stresses on the forest in addition to continued warming (Bush et al., 2016; Gloor et al., 2015). For example, severe drought in Indonesia facilitates large fires and increased land use (Field et al., 2009); similarly, the synergies of multi-year drought and associated increased forest flammability combined with increased land use pressure, could exacerbate land conversion challenges in the Amazonian forest. Thus, the threats to Amazonian biodiversity, carbon storage, water cycling, and other critical forest services could be significantly larger than previously anticipated given the combination of multi-year drought and inevitable warming.

Acknowledgments, Samples, and Data

We thank the NSF Amazon-PIRE program, the Kartchner Caverns scholarship fund, and the Department of Geosciences at the University of Arizona for their funding support. The Paleoecology Lab at the Florida Institute of Technology, and especially Bryan Valencia, were also critical to the success of this research. This material is based upon work supported by the National Science Foundation grants EAR1304083 and EaSM2 AGS1243125, as well as a NSF Graduate Research Fellowship under Grant DGE-1143953. Sea-surface temperature and precipitation data provided by the NOAA/OAR/ESRL PSD, Boulder, Colorado, USA, from their Web site at http://www.esrl.noaa.gov/psd/. Data from CMIP5 on https://pcmdi9.llnl.gov/search/cmip5/, paleoclimate data available at http://www.ncdc.noaa.gov/paleo/. Lake Limón μ-XRF elemental time series and principal

component time series are available at the NOAA Paleoclimatology Data website: www.ncdc.noaa.gov/data-access/paleoclimatology-data.

References

Adler, R. et al. (2003), The version-2 global precipitation climatology project (GPCP) monthly precipitation analysis (1979-present), *J. Hydrometeorol., 4*, 1147-1167.

Apaestegui, J. et al. (2014), Hydroclimate variability of the northwestern Amazon Basin near the Andean foothills of Peru related to the South American Monsoon System during the last 1600 years, *Clim. Past., 10*, 1967-1981.

Appleby, P. (2002), Chronostratigraphic techniques in recent sediments, *Tracking Environmental Change using Lake Sediments, Vol 1: Basin Analysis, Coring, and Chronological Techniques, 1*, 171-203.

Appleby, P. and F. Oldfield (1983), The Assessment of Pb-210 Data from Sites with Varying Sediment Accumulation Rates, *Hydrobiologia, 103*, 29-35.

Aragão, L. E., L. O. Anderson, M. G. Fonseca, T. M. Rosan, L. B. Vedovato, F. H. Wagner, C. V. Silva, C. H. S. Junior, E. Arai, and A. P. Aguiar (2018), 21st Century drought-related fires counteract the decline of Amazon deforestation carbon emissions, *Nature Communications*, 9, 536.

Ault, T. R., J. E. Cole, and S. S. George (2012), The amplitude of decadal to multidecadal variability in precipitation simulated by state-of-the-art climate models, *Geophys. Res. Lett., 39*, L21705.

Ault, T. R., J. E. Cole, J. T. Overpeck, G. T. Pederson, and D. M. Meko (2014), Assessing the Risk of Persistent Drought Using Climate Model Simulations and Paleoclimate Data, *J. Clim., 27*, 7529-7549.

Ault, T. R., J. E. Cole, J. T. Overpeck, G. T. Pederson, S. St George, B. Otto-Bliesner, C. A. Woodhouse, and C. Deser (2013), The Continuum of Hydroclimate Variability in Western North America during the Last Millennium, *J. Clim., 26*, 5863-5878.

Balascio, N. L. and R. S. Bradley (2012), Evaluating Holocene climate change in northern Norway using sediment records from two contrasting lake systems, *J. Paleolimnol*., 48, 259-273.

Balascio, N. L., Z. Zhang, R. S. Bradley, B. Perren, S. O. Dahl, and J. Bakke (2011), A multi-proxy approach to assessing isolation basin stratigraphy from the Lofoten Islands, Norway, *Quatern. Res*., 75, 288-300.

Ballantyne, A. P., P. A. Baker, J. Q. Chambers, R. Villalba, and J. Argollo (2011), Regional Differences in South American Monsoon Precipitation Inferred from the Growth and Isotopic Composition of Tropical Trees, *Earth Interact., 15*, 5.

Bird, B. W., M. B. Abbott, M. Vuille, D. T. Rodbell, N. D. Stansell, and M. F. Rosenmeier (2011), A 2,300-year-long annually resolved record of the South American summer monsoon from the Peruvian Andes, *Proc. Natl. Acad. Sci. U. S. A., 108*, 8583-8588.

Blaauw, M. (2010), Methods and code for 'classical' age-modelling of radiocarbon sequences, *Quat. Geochronol., 5*, 512-518.

Black, D. E., M. A. Abahazi, R. C. Thunell, A. Kaplan, E. J. Tappa, and L. C. Peterson (2007), An 8-century tropical Atlantic SST record from the Cariaco Basin: Baseline variability, twentieth-century warming, and Atlantic hurricane frequency, *Paleoceanography, 22*, PA4204.

Boening, P., E. Bard, and J. Rose (2007), Toward direct, micron-scale XRF elemental maps and quantitative profiles of wet marine sediments, *Geochem. Geophys. Geosyst., 8*, Q05004.

Boers, N., N. Marwan, H. M. Barbosa, and J. Kurths (2017), A deforestation-induced tipping point for the South American monsoon system, *Sci. Rep., 7*, 41489.

Brando, P. M. et al. (2014), Abrupt increases in Amazonian tree mortality due to drought–fire interactions, *Proceedings of the National Academy of Sciences, 111*, 6347-6352.

Brienen, R. J. W., G. Helle, T. L. Pons, J. Guyot, and M. Gloor (2012), Oxygen isotopes in tree rings are a good proxy for Amazon precipitation and El Nino-Southern Oscillation variability, *Proc. Natl. Acad. Sci. U. S. A., 109*, 16957-16962.

Brohan, P., J. J. Kennedy, I. Harris, S. F. B. Tett, and P. D. Jones (2006), Uncertainty estimates in regional and global observed temperature changes: A new data set from 1850, *J. Geophys. Res. -Atmos., 111*, D12106.

Bush, M. B., A. Correa -Metrio, R. W
disturbance amplifies Amazonian El Niño–Southern Oscillation signal, *Global Change Biol.*

Bush, M. B., A. Correa-Metrio, C. H. McMichael, S. Sully, C. R. Shadik, B. G. Valencia, T. Guilderson, M. Steinitz-Kannan, and J. T. Overpeck (2016), A 6900-year history of landscape modification by humans in lowland Amazonia, *Quat. Sci. Rev., 141*, 52-64.

Christensen, J. H. and et al. (2013), Climate Phenomena and their Relevance for Future Regional Climate Change. In: Climate Change 2013: The Physical Science Basis. Contribution of Working Group I to the Fifth Assessment Report of the Intergovernmental Panel on Climate Change.

Clark, J. S. and P. D. Royall (1996), Local and regional sediment charcoal evidence for fire regimes in presettlement north-eastern North America, *J. Ecol.*, 365-382.

Cohen, A. S. (Ed.) (2003), *Paleolimnology: The History and Evolution of Lake Systems*, Oxford University Press.

Colombaroli, D. and D. G. Gavin (2010), Highly episodic fire and erosion regime over the past 2,000 y in the Siskiyou Mountains, Oregon, *Proc. Natl. Acad. Sci. U. S. A.*, *107*, 18909-18914.

Correa-Metrio, A., K. R. Cabrera, and M. B. Bush (2010), Quantifying ecological change through discriminant analysis: a paleoecological example from the Peruvian Amazon, *J. Veg. Sci.*, *21*, 695-704.

Cox, P. M., R. A. Betts, M. Collins, P. P. Harris, C. Huntingford, and C. D. Jones (2004), Amazonian forest dieback under climate-carbon cycle projections for the 21st century, *Theoretical and Applied Climatology*, *78*, 137-156.

Cox, P. M., P. P. Harris, C. Huntingford, R. A. Betts, M. Collins, C. D. Jones, T. E. Jupp, J. A. Marengo, and C. A. Nobre (2008), Increasing risk of Amazonian drought due to decreasing aerosol pollution, *Nature*, *453*, 212-U7.

Dai, A. (2013), Increasing drought under global warming in observations and models, *Nature Climate Change*, *3*, 52-58.

Davidson, E. and et al. (2012), Climate Change, Deforestation, and the Fate of the Amazon, *Nature*, *481*, 321-328.

Davies, S. J., H. F. Lamb, and S. J. Roberts (2015), Micro-XRF core scanning in palaeolimnology: Recent developments, in Micro-XRF Studies of Sediment Cores, pp. 189-226, Springer.

Dee, S., L. Parsons, G. Loope, J. Overpeck, T. Ault, and J. Emile-Geay (2017), Improved spectral comparisons of paleoclimate models and observations via proxy system modeling: Implications for multi-decadal variability, *Earth Planet. Sci. Lett.*, 476, 34-46.

Diffenbaugh, N. S. and F. Giorgi (2012), Climate change hotspots in the CMIP5 global climate model ensemble, *Clim. Change*, *114*, 813-822.

Dirzo, R. and P. H. Raven (2003), Global state of biodiversity and loss, *Annual Review of Environment and Resources*, *28*, 137-167.

Espinoza, J. C., J. Ronchail, J. L. Guyot, C. Junquas, P. Vauchel, W. Lavado, G. Drapeau, and R. Pombosa (2011), Climate variability and extreme drought in the upper Solimões River (western Amazon Basin): Understanding the exceptional 2010 drought, *Geophys. Res. Lett.*, 38.

Espinoza, J. C., S. Chavez, J. Ronchail, C. Junquas, K. Takahashi, and W. Lavado (2015), Rainfall hotspots over the southern tropical Andes: Spatial distribution, rainfall intensity, and relations with large scale atmospheric circulation, *Water Resour. Res.*, 51, 3459-3475.

Espinoza, J. C., H. Segura, J. Ronchail, G. Drapeau, and O. Gutierrez -Cori (2016), E
wet -day and dry- day fre
atmospheric circulation and impacts on vegetation, *Water Resour. Res.*, 52, 8546-8560.

Fernandes, K., A. Giannini, L. Verchot, W. Baethgen, and M. Pinedo-Vasquez (2015), Decadal covariability of Atlantic SSTs and western Amazon dry-season hydroclimate in observations and CMIP5 simulations, *Geophys. Res. Lett.*, 42, 6793-6801.

Field, R. D., Van Der Werf, Guido R, and S. S. Shen (2009), Human amplification of drought-induced biomass burning in Indonesia since 1960, *Nature Geoscience, 2*, 185-188.

Gloor, M., L. Gatti, R. Brienen, T. Feldpausch, O. Phillips, J. Miller, J. Ometto, H. Rocha, T. Baker, and B. De Jong (2012), The carbon balance of South America: a review of the status, decadal trends and main determinants, *Biogeosciences, 9*, 5407-5430.

Gloor, M., J. Barichivich, G. Ziv, R. Brienen, J. Schöngart, P. Peylin, B. B. Ladvocat Cintra, T. Feldpausch, O. Phillips, and J. Baker (2015), Recent Amazon climate as background for possible ongoing and future changes of Amazon humid forests, *Global Biogeochem. Cycles, 29*, - 2014GB005080.

Gray, S., L. Graumlich, J. Betancourt, and G. Pederson (2004), A tree-ring based reconstruction of the Atlantic Multidecadal Oscillation since 1567 AD, *Geophys. Res. Lett., 31*, L12205.

Guimberteau, M., J. Ronchail, J. Espinoza, M. Lengaigne, B. Sultan, J. Polcher, G. Drapeau, J. Guyot, A. Ducharne, and P. Ciais (2013), Future changes in precipitation and impacts on extreme streamflow over Amazonian sub-basins, *Environmental Research Letters*, 8, 014035.

Haberzettl, T., M. Fey, A. Lücke, N. Maidana, C. Mayr, C. Ohlendorf, F. Schäbitz, G. H. Schleser, M. Wille, and B. Zolitschka (2005), Climatically induced lake level changes during the last two millennia as reflected in sediments of Laguna Potrok Aike, southern Patagonia (Santa Cruz, Argentina*), J. Paleolimnol*., 33, 283-302.

Haug, G., K. Hughen, D. Sigman, L. Peterson, and U. Rohl (2001), Southward migration of the intertropical convergence zone through the Holocene, *Science, 293*, 1304-1308.

Hedges, R., I. Law, C. Bronk, and R. Housley (1989), The Oxford Accelerator Mass-Spectrometry Facility - Technical Developments in Routine Dating, *Archaeometry, 31*, 99-113.

HidroWeb, Sistema de Informacoes Hidrologicas, Agencia Nacional de Aguas (ANA), 2003, http://hidroweb.ana.gov.br/default.asp.

Huang, B., V. F. Banzon, E. Freeman, J. Lawrimore, W. Liu, T. C. Peterson, T. M. Smith, P. W. Thorne, S. D. Woodruff, and H. Zhang (2015), Extended Reconstructed Sea Surface Temperature Version 4 (ERSST.v4). Part I: Upgrades and Intercomparisons, *J. Clim., 28*, 911-930.

Jimenez-Munoz, J. C., C. Mattar, J. Barichivich, A. Santamaria-Artigas, K. Takahashi, Y. Malhi, J. A. Sobrino, and G. van der Schrier (2016), Record-breaking warming and extreme drought in the Amazon rainforest during the course of El Nino 2015-2016, *Sci Rep, 6*, 33130.

Kanner, L. C., S. J. Burns, H. Cheng, R. L. Edwards, and M. Vuille (2013), High-resolution variability of the South American summer monsoon over the last seven millennia: insights from a speleothem record from the central Peruvian Andes, *Quat. Sci. Rev., 75*, 1-10.

Lenton, T. M., H. Held, E. Kriegler, J. W. Hall, W. Lucht, S. Rahmstorf, and H. J. Schellnhuber (2008), Tipping elements in the Earth's climate system, *Proc. Natl. Acad. Sci. U. S. A., 105*, 1786-1793.

Lewis, S. L., P. M. Brando, O. L. Phillips, G. M. F. van der Heijden, and D. Nepstad (2011), The 2010 Amazon Drought, *Science, 331*, 554-554.

Li, W., P. Zhang, J. Ye, L. Li, and P. A. Baker (2011), Impact of two different types of El Niño events on the Amazon climate and ecosystem productivity, *Journal of Plant Ecology*, 4, 91-99.

Lomb, N. (1975), Spectrographic Study of Beta-Centauri, *Mon. Not. Roy. Astron. Soc., 172*, 639-647.

Malhi, Y., L. E. O. C. Aragao, D. Galbraith, C. Huntingford, R. Fisher, P. Zelazowski, S. Sitch, C. McSweeney, and P. Meir (2009), Exploring the likelihood and mechanism of a climate-change-induced dieback of the Amazon rainforest, *Proc. Natl. Acad. Sci. U. S. A., 106*, 20610-20615.

Malhi, Y., J. T. Roberts, R. A. Betts, T. J. Killeen, W. Li, and C. A. Nobre (2008), Climate change, deforestation, and the fate of the Amazon, *Science, 319*, 169-172.

Marengo, J. and J. Espinoza (2016), Extreme seasonal droughts and floods in Amazonia: causes, trends and impacts, *Int. J. Climatol., 36*, 1033-1050.

Matthews-Bird, F., B. G. Valencia, W. Church, L. C. Peterson, and M. Bush (2017), A 2000-year history of disturbance and recovery at a sacred site in Peru's northeastern cloud forest, *The Holocene*, 27, 1707-1719.

McCormac, F., A. Hogg, P. Blackwell, C. Buck, T. Higham, and P. Reimer (2004), SHCal04 Southern Hemisphere calibration, 0-11.0 cal kyr BP, *Radiocarbon, 46*, 1087-1092.

Metcalfe, S. E., M. Jones, S. J. Davies, A. Noren, and A. MacKenzie (2010), Climate variability over the last two millennia in the North American Monsoon region, recorded in laminated lake sediments from Laguna de Juanacatlán, Mexico, *The Holocene*, 20, 1195-1206.

Mittermeier, R. A., N. Myers, J. B. Thomsen, G. A. Da Fonseca, and S. Olivieri (1998), Biodiversity hotspots and major tropical wilderness areas: approaches to setting conservation priorities, *Conserv. Biol., 12*, 516-520.

Moreno, A., S. Giralt, B. Valero-Garces, A. Saez, R. Bao, R. Prego, J. J. Pueyo, P. Gonzalez-Samperiz, and C. Taberner (2007), A 14 kyr record of the tropical Andes: The Lago Chungara sequence (18 degrees S, northern Chilean Altiplano), *Quaternary International, 161*, 4-21.

Nepstad, D., C. et al. (1994), The Role of Deep Roots in the Hydrological and Carbon Cycles of Amazonian Forests and Pastures, *Nature, 372*, 666-669.

Niemann, H., T. Haberzettl, and H. Behling (2009), Holocene climate variability and vegetation dynamics inferred from the (11700 cal. yr BP) Laguna Rabadilla de Vaca sediment record, southeastern Ecuadorian Andes, *Holocene, 19*, 307-316.

North, G. R., T. L. Bell, R. F. Cahalan, and F. J. Moeng (1982), Sampling errors in the estimation of empirical orthogonal functions, *Mon. Weather Rev.*, 110, 699-706.

Novello, V. F. et al. (2012), Multidecadal climate variability in Brazil's Nordeste during the last 3000 years based on speleothem isotope records, *Geophys. Res. Lett., 39*, L23706.

Novello, V. F. et al. (2016), Centennial-scale solar forcing of the South American Monsoon System recorded in stalagmites, *Sci Rep, 6*, 24762.

Parsons, L. A., G. R. Loope, J. T. Overpeck, T. R. Ault, R. Stouffer, and J. E. Cole (2017), Temperature and precipitation variance in CMIP5 simulations and paleoclimate records of the last millennium, *J. Clim.*

Phillips, O. L. et al. (2009), Drought Sensitivity of the Amazon Rainforest, *Science, 323*, 1344-1347.

Pike, J. and A. E. S. Kemp (1996), Preparation and analysis techniques for studies of laminated sediments, *Geological Society, London, Special Publications, 116*, 37-48.

Reuter, J., L. Stott, D. Khider, A. Sinha, H. Cheng, and R. L. Edwards (2009), A new perspective on the hydroclimate variability in northern South America during the Little Ice Age, *Geophys. Res. Lett., 36*, L21706.

Ronchail, J., G. Cochonneau, M. Molinier, J. Guyot, A. Chaves, V. Guimaraes, and E. de Oliveira (2002), Interannual rainfall variability in the Amazon basin and sea-surface temperatures in the equatorial Pacific and the tropical Atlantic Oceans, *Int. J. Climatol., 22*, 1663-1686.

Rojas, M. et al. (2016), The South American monsoon variability over the last millennium in climate models, *Climate of the Past*, 12, 1681.

Saatchi, S., S. Asefi-Najafabady, Y. Malhi, L. E. O. C. Aragao, L. O. Anderson, R. B. Myneni, and R. Nemani (2013), Persistent effects of a severe drought on Amazonian forest canopy, *Proc. Natl. Acad. Sci. U. S. A., 110*, 565-570.

Scargle, J. (1982), Studies in Astronomical Time-Series Analysis.2. Statistical Aspects of Spectral-Analysis of Unevenly Spaced Data, *Astrophys. J., 263*, 835-853.

Schmidt, G. A. et al. (2012), Climate forcing reconstructions for use in PMIP simulations of the Last Millennium (v1.1), *Geosci. Model Dev., 5*, 185-191.

Schneider, U., A. Becker, P. Finger, A. Meyer-Christoffer, M. Ziese, and B. Rudolf (2014), GPCC's new land surface precipitation climatology based on quality-controlled in situ data and its role in quantifying the global water cycle, *Theor. Appl. Climatol., 115*, 15-40.

Shala, S., K. F. Helmens, K. N. Jansson, M. E. Kylander, J. Risberg, and L. Löwemark (2014), Palaeoenvironmental record of glacial lake evolution during the early Holocene at Sokli, NE Finland, *Boreas*, 43, 362-376.

Shanahan, T. M., J. T. Overpeck, J. B. Hubeny, J. King, F. S. Hu, K. Hughen, G. Miller, and J. Black (2008), Scanning micro-X-ray fluorescence elemental mapping: A new tool for the study of laminated sediment records, *Geochem. Geophys. Geosyst., 9*, Q02016.

Shanahan, T. M., J. T. Overpeck, K. J. Anchukaitis, J. W. Beck, J. E. Cole, D. L. Dettman, J. A. Peck, C. A. Scholz, and J. W. King (2009), Atlantic forcing of persistent drought in West Africa, *Science*, 324, 377-380.

Taylor, K. E., R. J. Stouffer, and G. A. Meehl (2012), An Overview of CMIP5 and the Experiment Design, *Bull. Am. Meteorol. Soc., 93*, 485-498.

Thompson, L. G., E. Mosley-Thompson, M. E. Davis, V. S. Zagorodnov, I. M. Howat, V. N. Mikhatenko, and P. -. Lin (2013), Annually Resolved Ice Core Records of Tropical Climate Variability over the Past similar to 1800 Years, *Science, 340*, 945-950.

Tian, H., J. M. Melillo, D. W. Kicklighter, A. D. McGuire, J. V. Helfrich, B. Moore, and C. J. VoÈroÈsmarty (1998), Effect of interannual climate variability on carbon storage in Amazonian ecosystems, *Nature, 396*, 664-667.

Van Albada, S. and P. Robinson (2007), Transformation of arbitrary distributions to the normal distribution with application to EEG test–retest reliability, *J. Neurosci. Methods*, 161, 205-211.

Vera, C. et al. (2006), Toward a unified view of the American Monsoon Systems, *J. Clim., 19*, 4977-5000.

Vuille, M., S. J. Burns, B. L. Taylor, F. W. Cruz, B. W. Bird, M. B. Abbott, L. C. Kanner, H. Cheng, and V. F. Novello (2012), A review of the South American monsoon history as recorded in stable isotopic proxies over the past two millennia, *Clim. Past.*, 8, 1309-1321.

Yin, L., R. Fu, E. Shevliakova, and R. E. Dickinson (2013), How well can CMIP5 simulate precipitation and its controlling processes over tropical South America?, *Clim. Dyn.,* 41, 3127-3143.

Yoon, J. and N. Zeng (2010), An Atlantic influence on Amazon rainfall, *Clim. Dyn., 34*, 249-264.

Zemp, D. C., C. Schleussner, H. M. Barbosa, M. Hirota, V. Montade, G. Sampaio, A. Staal, L. Wang-Erlandsson, and A. Rammig (2017), Self-amplified Amazon forest loss due to vegetation-atmosphere feedbacks, *Nature Communications, 8*, 14681.

Zhou, J. and K. Lau (1998), Does a monsoon climate exist over South America?, *J. Clim., 11*, 1020-1040.

Table 1

Data Sources, Locations, Temporal Coverage, and Relationships with Lake Limón Principal Components 1 and 2

Data	Source	Correlation PC1	Correlation PC2	Lat.(ºN)	Lon.(ºE)	Alt.(m)	Time (CE) Start:End
Trop. N. Atlantic	NOAAERSSTv4	***-0.56***	0.31	6:22	-80:-15	N/A	1854:2014
Niño3.4	NOAAERSSTv4	-0.15	-0.25	-5:5	-170:-120	N/A	1854:2014
Local Precipitation	GPCCv7	***0.60***	0.37	-7	-76	600	1901:2014
Rio Negro Flow	HidroWeb/Manaus	0.13	-0.08	-3.13	-60.01	10	1902:2015
N. Atl. SST Recon.	Gray et al.	-0.21	**-0.27**	0:70	N/A	N/A	1567:1990
Palestina $\delta^{18}O$	Apaestegui et al.	0.12	0.06	-5.92	-77.35	870	421:1928
Cascayunga $\delta^{18}O$	Reuter et al.	***0.26***	0.07	-6.07	-77.18	900	1088:1907
Sauce Redness	Bush et al.	**-0.14**	***-0.26***	-6.71	-76.23	600	-3054:1999
Limón Elemental	Parsons et al.	N/A	N/A	-6.71	-76.23	600	564:1972
Cariaco SST	Black et al.	0.13	***0.23***	10.76	-64.70	-450	1221:1990
Cariaco %Ti	Haug et al.	0.19	0.12	10.70	-65.16	-893	-12327:1840
Pumacocha $\delta^{18}O$	Bird et al.	-0.01	***-0.15***	-10.71	-76.06	4300	-277:2007
Huagapo $\delta^{18}O$	Kanner et al.	0.08	**-0.15**	-11.27	-75.79	3850	559:2000
Tree $\delta^{18}O$ (Bolivia)	Brienen et al.	-0.42	-0.06	-11.40	-68.72	240	1901:2001
Quelccaya $\delta^{18}O$	Thompson et al.	0.06	0.09	-13.93	-70.83	5670	226:2009
Diva de Maura $\delta^{18}O$	Novello et al.	**-0.17**	**0.16**	-12.37	-41.57	680	-815:1911
Tree $\delta^{18}O$ (Peru)	Ballantyne et al.	-0.04	0.22	-12.60	-69.20	265	1820:2004
Pau d'Alho $\delta^{18}O$	Novello et al.	0.07	0.11	-15.21	-56.81	540	492:1860

Table 2

Principal Components and Elemental Constituent Correlations

Significant correlations between elements and principal components shown in bold font (North et al., 1982). Percent variance explained by each principal component shown in parentheses.

Element	PC1(40%)	PC2(28%)	PC3(16%)
Al	**0.92**	**-0.32**	**-0.50**
Si	**0.28**	**0.12**	**-0.92**
S	**0.10**	**-0.95**	0.05
K	**0.54**	**-0.12**	**-0.81**
Ca	**-0.43**	**-0.19**	-0.02
Ti	**0.92**	**-0.27**	**-0.23**
Mn	**-0.11**	**-0.42**	-0.01
Fe	**0.68**	**-0.85**	0.03
Rb	**0.92**	**-0.34**	**-0.21**
Sr	-0.03	**-0.25**	**0.36**

Figure Captions

Figure 1. Maps showing regional climatology and paleoclimate record locations, local topography, and Lake Limón bathymetry. (a) Map of satellite-era September to March South American GPCP v2.3 precipitation (Adler et al., 2003) and paleoclimate record locations (citations and other record information in Table 1). Red line outlines Amazon River drainage basin and filled red square indicates Lake Limón location. (b) Contour map of basin around Lake Limón. (c) Bathymetric map (blue shading) of Lake Limón with orange circles marking coring locations.

Figure 2. Lake Limón stratigraphy and age model, including radiocarbon and ^{210}Pb ages. "Best fit" age model produced in *clam* with a 2-σ age envelope. Dates in blue were used to create the final age model. Dates in tan were excluded due to small size. Dates in green were considered outliers and thus excluded. Dates in dark gray were taken on bulk sediment and were thus excluded. Inset shows ^{210}Pb dates with 1-σ error bars.

Figure 3: Correlation between sea-surface temperature and September-March interannual precipitation. (a) Tropical North Atlantic (NAtl) SST and September-March precipitation and (b) Niño3.4 SST and September-March precipitation 1901-2014CE. Red box marks location of Lake Limón, red line outlines the Amazon River drainage basin, and black dots indicate correlations at the 95% significance level. All correlations calculated using 5-year bins to match with proxy-observation correlation analysis.

Figure 4: Correlations between Lake Limón PC1 and observations of precipitation and sea-surface temperatures. (a) Correlation coefficient between Lake Limón PC1 and September-March GPCCv7 (Schneider et al., 2014) precipitation (5-year bins). (b) Correlation coefficient between Lake Limón PC1 and annual mean NOAA ERSSTv4 (Huang et al., 2015) sea-surface temperatures (5-year bins). Stippling in both panels marks regions with significant correlations ($p<0.05$). Correlations calculated during the time periods 1901-1972 CE (GPCCv7) and 1854-1972 CE (ERSSTv4). Red square in South America indicates the location of Lake Limón. Red line (a) outlines the Amazon drainage basin, and red box (b) outlines tropical North Atlantic region used for correlation with Lake Limón PC1. Scatter plot (c) shows the relationship between the 5-year binned Lake Limón PC1 and 5-year binned GPCCv7 precipitation anomalies (see Table 1 for region used to make GPCCv7 precipitation time series).

Figure 5: Lake Limón first principal component of elemental variation, Lake Limón charcoal count, tropical Atlantic SST, and local wet-season precipitation. (a) First principal component of Lake Limón hydroclimatic variability, plotted in black (5-year bins), tropical north Atlantic SST plotted in red (6-22ºN and 80-15ºW, 5-year bins), and wet-season precipitation plotted in blue (8º-7ºS, 77º-76ºE, 5-year bins, September-March, dashed line indicates poor data coverage before 1950CE). Correlation coefficients between Lake Limón and 5-year bins of each time

series shown above associated time series. (b) First principal component of Lake Limón hydroclimatic variability, plotted in black as a 5-year moving average, ~564 to 1972 CE. Long-term mean shown as dotted line at zero. Dark and light shaded boxes outline one and two standard deviations above and below the mean. Vertical shaded gray lines show dry periods below one standard deviation, vertical shaded brown lines show dry periods below two standard deviations, and vertical blue shaded lines show wet periods above one standard deviation in western Amazonia. Arrows indicate major elemental contributions to Lake Limón principal component. Lake Limón principal component and instrumental observations shown as 5-year bins to account for lake age model uncertainty. Charcoal concentration data (blue vertical bars; see Materials and Methods) shown in 40-year bins to account for age uncertainty associated with cross-core correlation within Lake Limón.

Figure 6. Lake Limón PC1 and simulated western Amazonian drought distributions over the last millennium. (a) CMIP5 precipitation drought distribution 1σ below 850-1850CE mean. (b) Lake Limón PC1 drought distribution 1σ below mean. (c) CMIP5 precipitation drought distribution 2σ below mean. (d) Lake Limón PC1 drought distribution 2σ below mean (Methods). Individual CMIP5 model minimum and maximum number of drought events shown with vertical lines in (a) and (c).

Figure 7. Lake Limón PC1, Amazonian paleoclimate mean, and CMIP5 precipitation power spectra. The Lake Limón PC1 spectrum is shown in black, the Amazonian paleoclimate spectral mean is shown in green, and the CMIP5 power spectra are shown in gray (control simulations) and red (transiently forced Last Millennium simulations). All spectral estimates plotted in evenly spaced frequency bins (spaced at equal 0.2 log intervals). Individual power spectra of Amazonian paleoclimate records shown in Figure S6.

Figure 8: Lake Limón PC1(black lines) and other tropical South American paleoclimate records (colored lines). (a) Palestina speleothem $\delta^{18}O$ (Apaestegui et al., 2014), (b) Laguna Sauce sediment redness (Bush et al., 2017), (c) Pau d'Alho speleothem $\delta^{18}O$ (Novello et al., 2016) (d) Cascayunga speleothem $\delta^{18}O$ (Reuter et al., 2009), (e) Cariaco Basin %Ti record (Haug et al., 2001), (f) NATL SST tree-ring reconstruction (Gray et al., 2004), and (g) Cariaco Basin Mg/Ca SST anomalies (Black et al., 2007). Note reversed axes on panels d, f, and g.

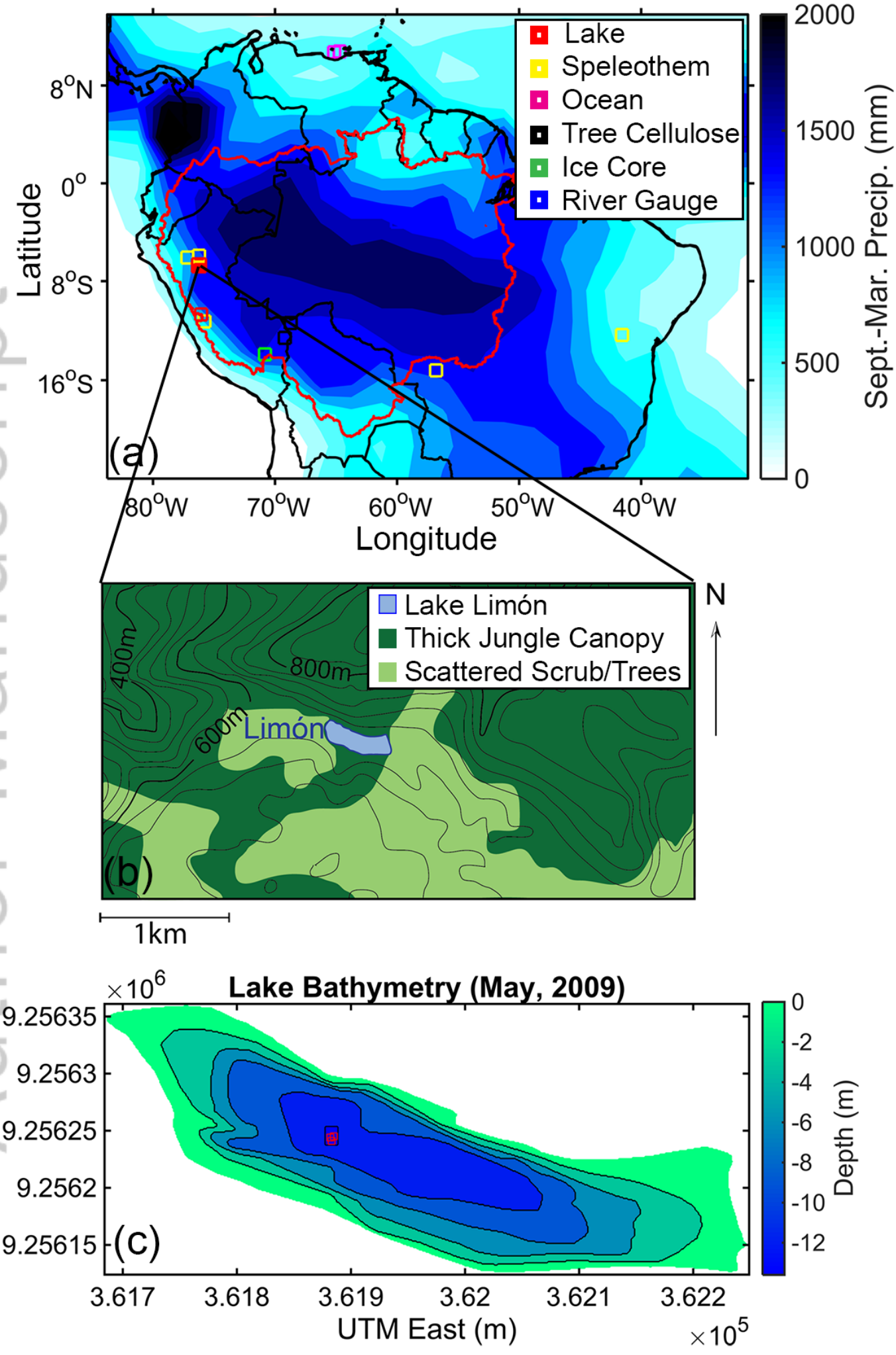

2017WR021788-f01-z-.png

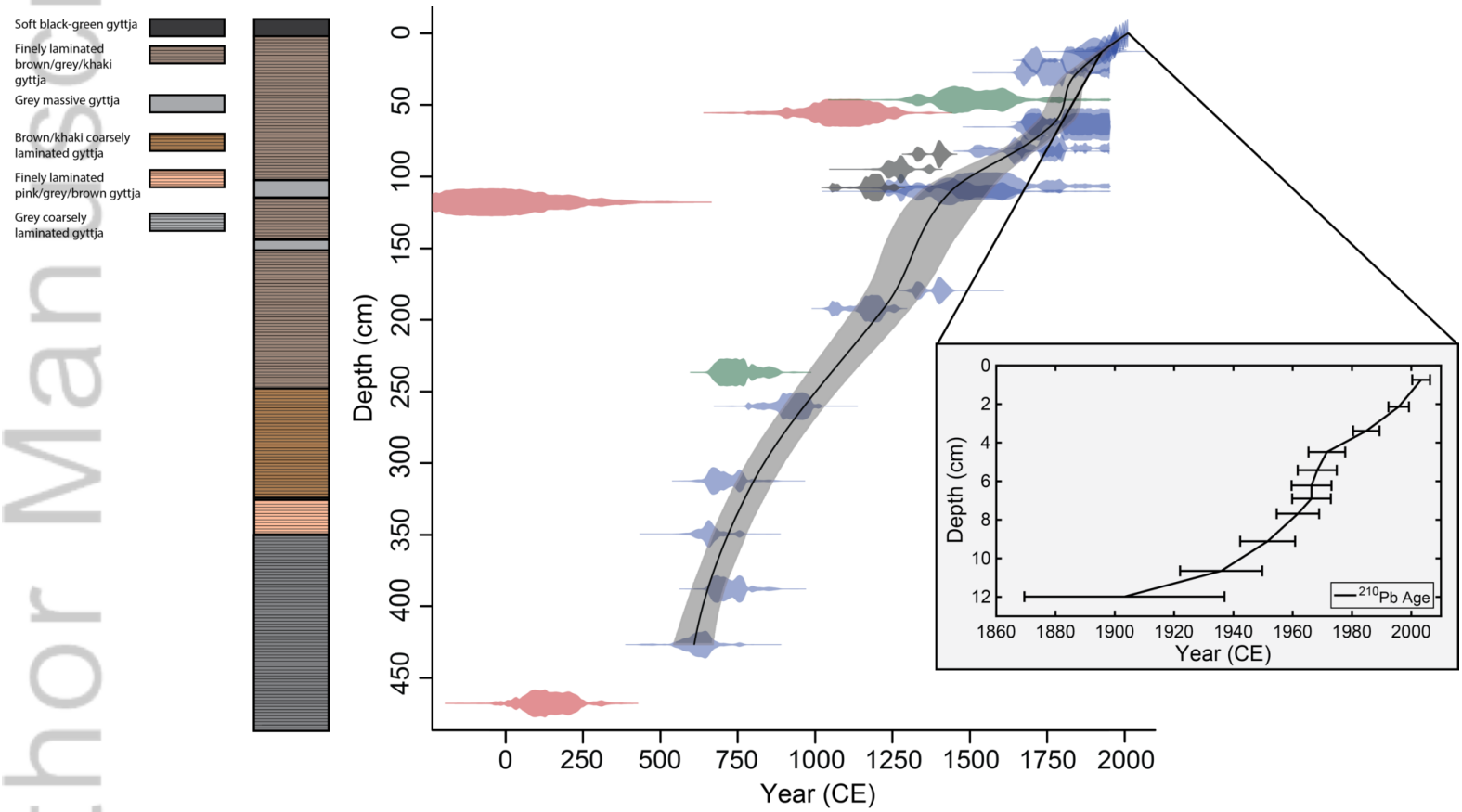

2017WR021788-f02-z-.png

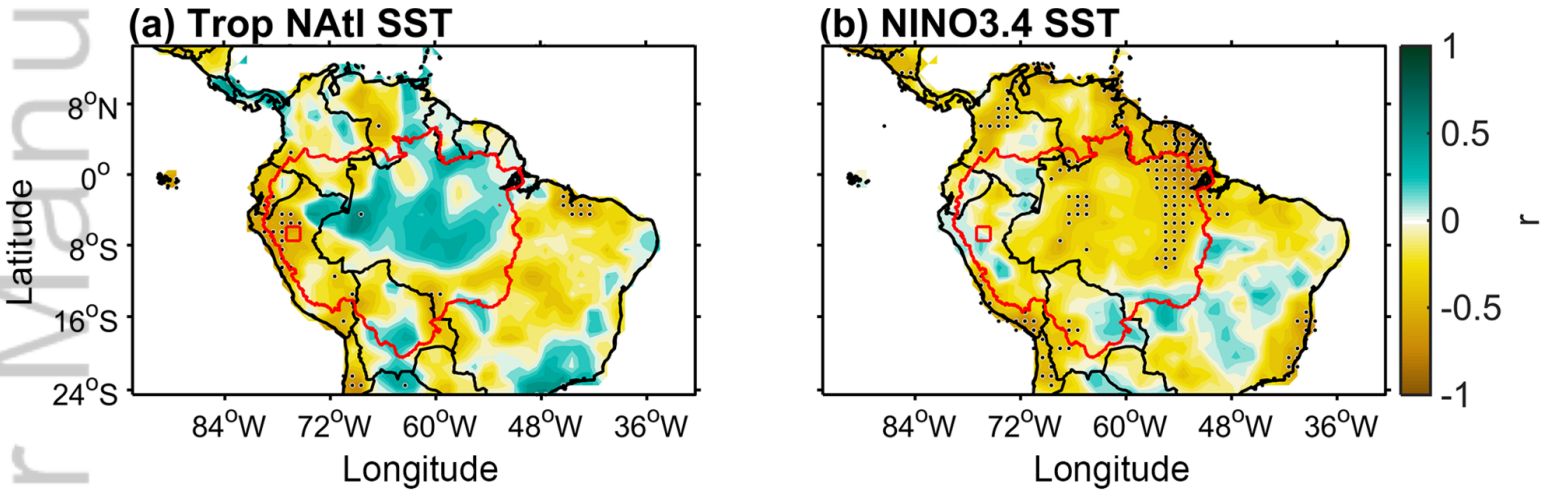

2017WR021788-f03-z-.png

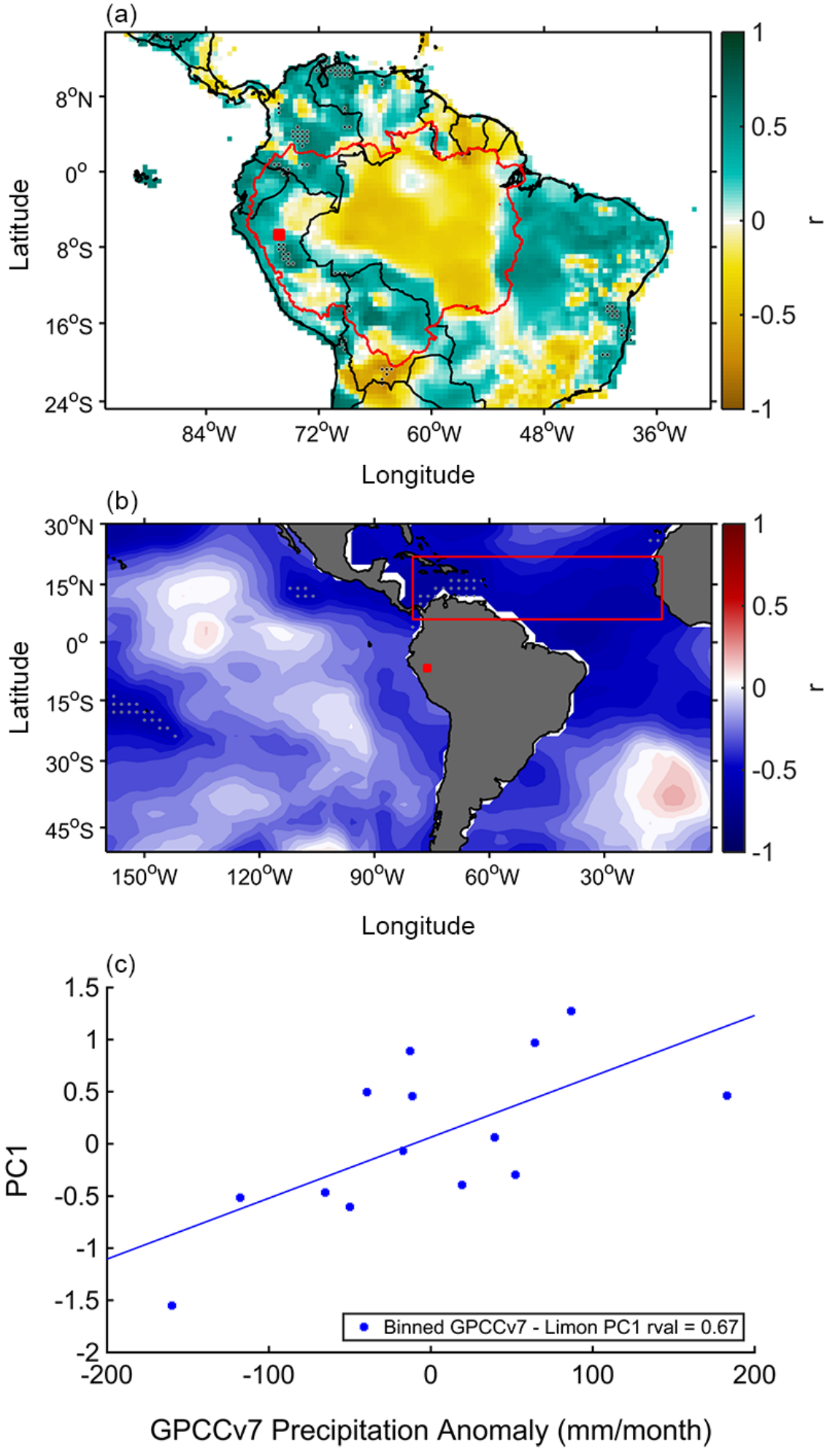

2017WR021788-f04-z-.png

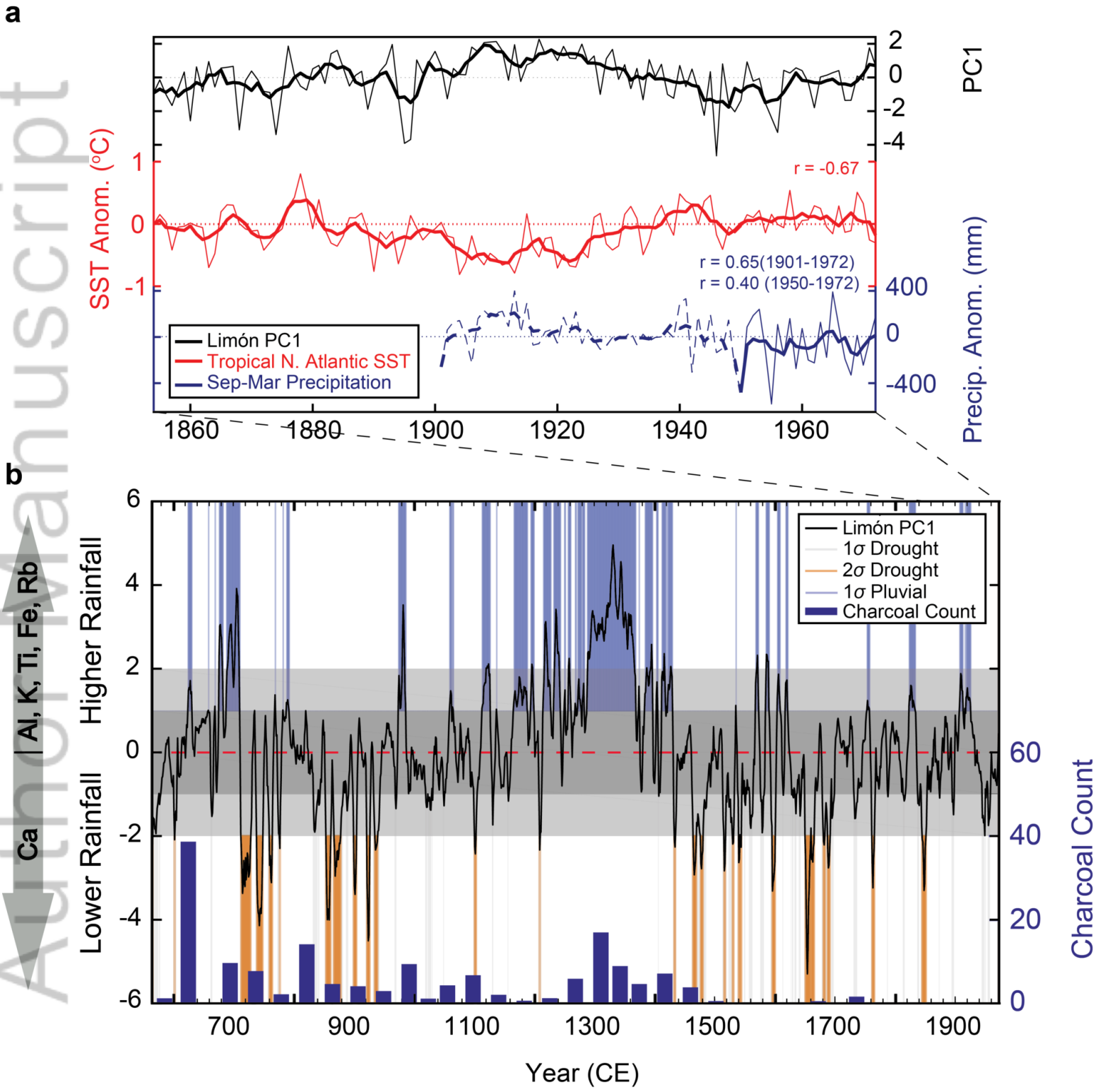

2017WR021788-f05-z-.png

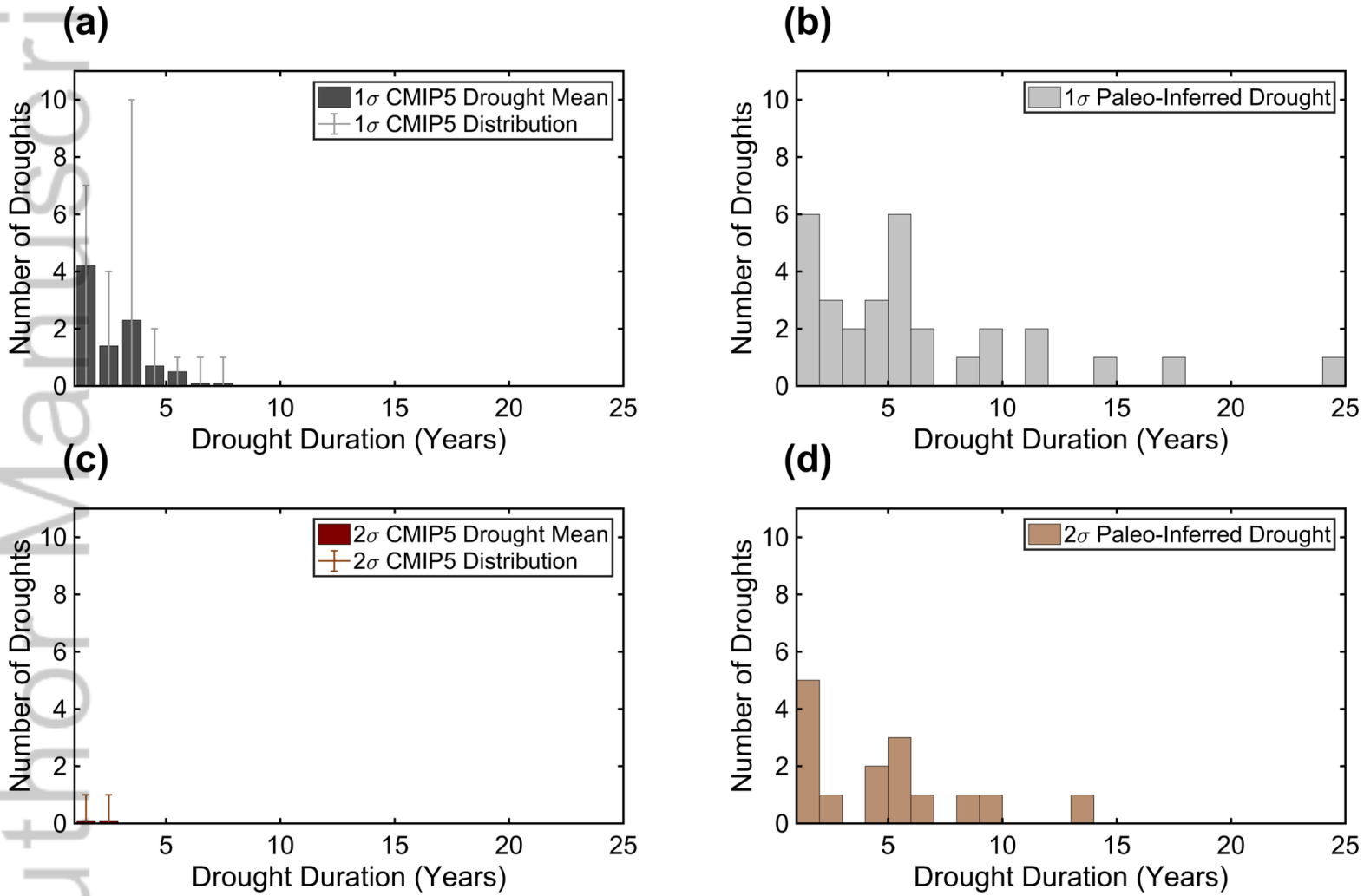

2017WR021788-f06-z-.png

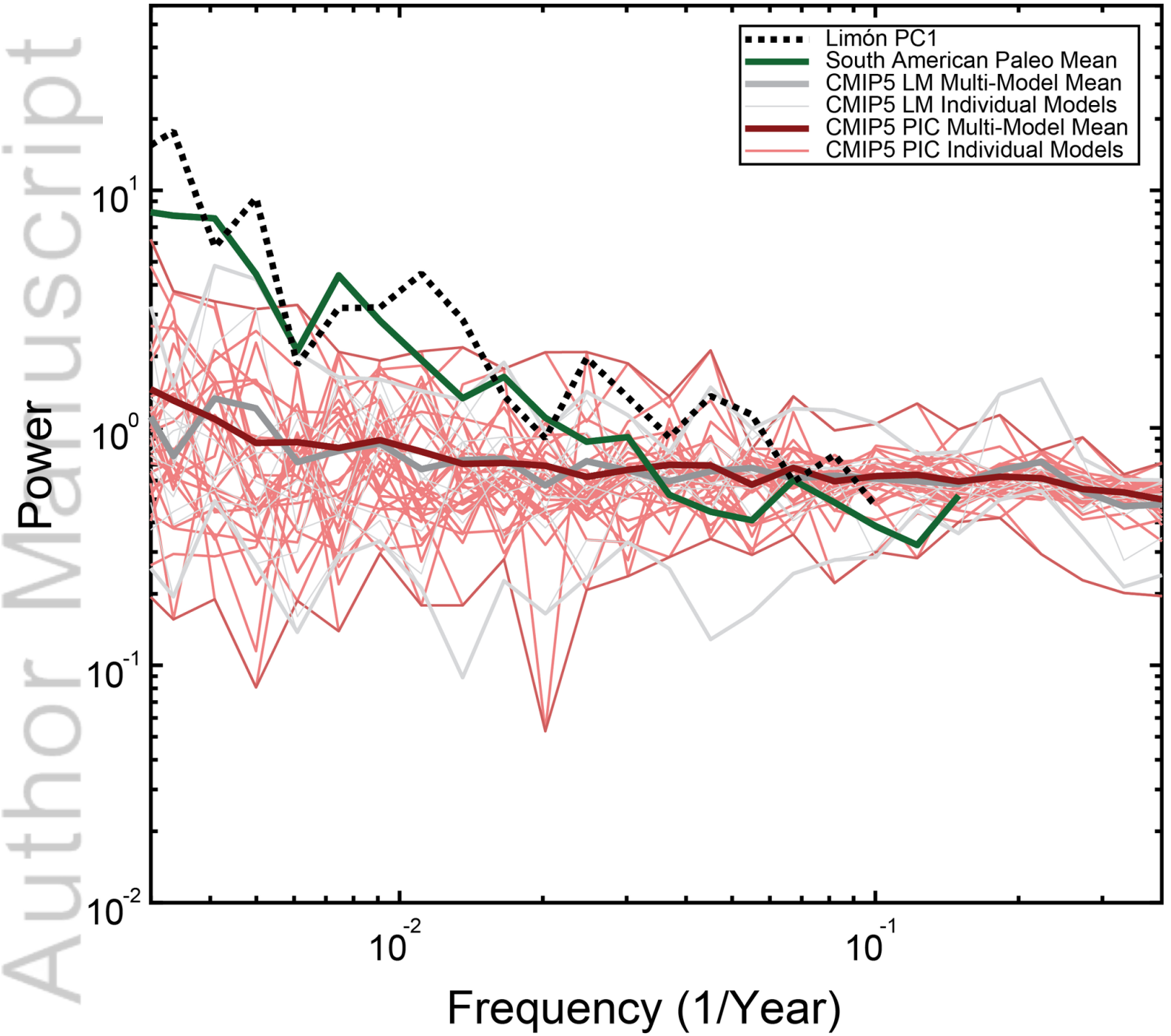

2017WR021788-f07-z-.png

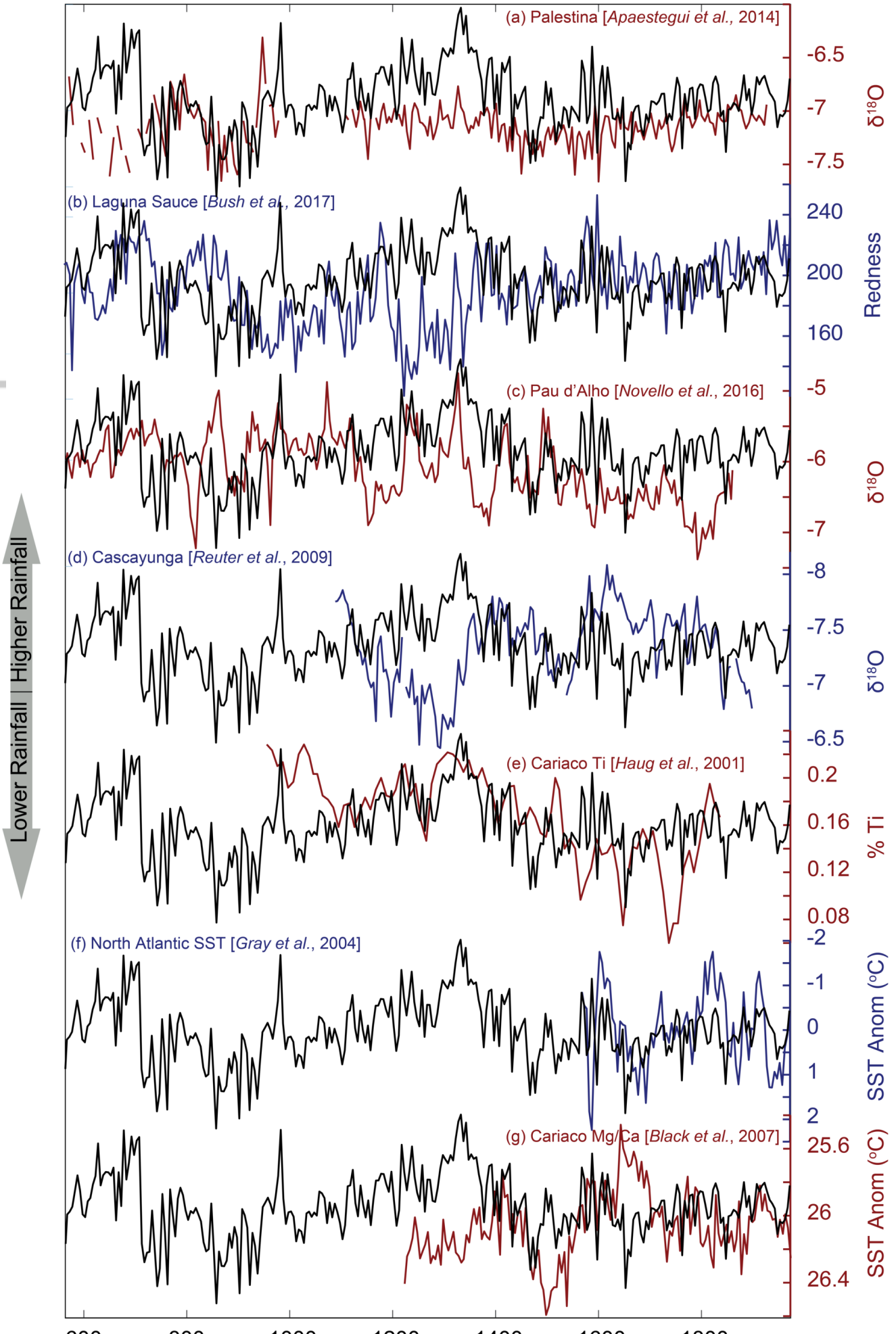

2017WR021788-f08-z-.png